Preparation of hydrodesulfurization catalysts using MoS_3 nanoparticles as a precursor

Yang Gao, Wei Han[*], Xiangyun Long, Hong Nie, Dadong Li

Research Institute of Petroleum Processing, SINOPEC, 18 Xue Yuan Road, 100083 Beijing, PR China

ABSTRACT

γ-Alumina-supported MoS_3 nanoparticles (NP_S) denoted as MoS_3/Al_2O_3 were firstly synthesized by chemical deposition method, and then used as the "second support" for promoter Ni atoms to prepare a pre-sulfided bimetallic HDS catalyst denoted as CAT-MoS_3 by the conventional impregnation method. Meanwhile, for comparison purpose, two bimetallic catalysts denoted as CAT-MoS_2 and CAT-MoO_3 with the same metal loadings were prepared using MoS_2/Al_2O_3 and MoO_3/Al_2O_3 as the starting material, respectively. Characterization and activity assessment show that, using MoS_3 as the precursor not only promotes the resulting bimetallic catalyst with a much higher sulfidation degree of Mo species, but also realizes a better decoration of Ni atoms onto the edges of MoS_2 nanoslabs. The dual effect guarantees the plentiful formation of Type II Ni-Mo-S active sites and thus remarkably enhances the hydrodesulfurization (HDS) activity. Compared with CAT-MoS_2, CAT-MoS_3 possesses very similar physical properties, microstructure and sulfidation degree of Mo species, however, due to its much higher decoration degree of Ni atoms, it holds a significantly enhanced HDS activity. Moreover, in comparison with CAT-MoS_2, CAT-MoO_3 exhibits a worse microstructure (more MoS_2 nanoslabs with larger length and lower stacking) and a much lower sulfidation degree of Mo species, but it still holds much higher HDS activity, further implying that the decoration degree (i.e. promoting effect) imposes the most important impact on the HDS activity. It is rational and effective to modify the starting state of Mo species to enhance the promoting effect and thereof improve the catalytic performance.

1. Introduction

In recent years, with the increasing supply of heavy feedstocks of decreasing quality and the more severe environmental regulations, the refineries are facing the more stringent tasks for producing cleaner oils with ultra-low sulfur content [1,2]. From a worldwide perspective, hydrodesulfurization (HDS) technologies will still be the most important way to produce vehicle fuel oils for a long time to come [3,4]. Due to the crucial role of catalysts in various HDS processes, developing catalysts with excellent performance has always been the most economical and effective way to achieve a deep HDS process [5].

MoS_2/WS_2 nano-crystallites decorated by Ni or/and Co atoms have generally been chosen as the active components of the hydrotreating catalysts since 1940's [6,7]. And due to the favorable combination of textural properties, acid/base characteristics and chemical and hydrothermal stability, γ-alumina and its modified ones are often applied as the support [8]. According to the widely accepted Co(Ni)-Mo-S active phase theory [9–12], there are two types of Co(Ni)-Mo-S phases: the type I is not fully sulfided and less stacked, strongly interacting with

alumina a Mo-O-Al bridges, whereas the type II phase is fully sulfided and highly stacked, exhibiting weak interaction through van der Waals force with alumina; the intrinsic activity of the later is two times higher than that of the former [13]. For Co or Ni atoms in Co(Ni)-Mo-S phase, they act as an electron donor through their electron-rich *d*-orbits. Once the edges of MoS_2 nanoslabs were decorated, the electron cloud density of the neighboring Mo atoms will be increased, which will increase the mobility of S atoms to induce the easier formation of the active coordinatively unsaturated sites (CUS) and thereby enhance the catalytic activity exponentially [9,14,15]. This electronic effect has been widely called "promoting effect" [16]. It is, accordingly, expected that an ideal HDS catalyst should be composed of type II CoMoS sites as many as possible [13]. Based on this, three aspects should be taken into account during the development of an excellent HDS catalyst, that is, (1) highly-dispersed Mo species; (2) fully-sulfided Mo species; and (3) well-decorated MoS_2 phases by Ni/Co promoter atoms.

During the industrial preparation of Mo-based hydrotreating catalysts, oxidic catalysts, such as $CoO(NiO)$-MoO_3/Al_2O_3 [17] and $CoO(NiO)$-MoO_3-P_2O_5/Al_2O_3 [18,19], are generally firstly prepared and

then reduced into the sulfided ones by using a mixture of a feed containing sulfur compounds and H_2 [19–22]. In short, oxidic Mo species are exploited as the active precursor of conventional hydrotreating catalysts. During impregnation, oxidic Mo-containing anions (such as $Mo_7O_{24}^{6-}$ and $P_2Mo_5O_{23}^{6-}$) are often used as the precursor of the above oxidic catalysts [18,23]. However, after being impregnated, dried and calcined, these anions will strongly interact with the alumina surface [9,24]. This interaction is beneficial to the dispersion of active species and thereby guarantees a high accessibility of the active sites to the reactants. However, it will lead to a non-ideal sulfidation degree of Mo species and thereof result in the formation of excess type I active sites [25,26]. In fact, it has always been a thorny problem to realize the Mo species with high dispersion and full sulfidation simultaneously through using the oxidic Mo species as the precursor. To overcome it, great efforts have been made to optimize the structure and composition of the precursors to obtain a series of new hybrid compounds, such as $Mo_4(C_6H_5O_7)_2O_{11}^{4-}$ [18], $[Mo_2O_4(C_2O_4)_2(H_2O)_2]^{2-}$ [27] and $Mo_8O_{26}[C_{12}H_{25}(CH_3)_3N]_4$ [26], which to an extent enhance the sulfidation degree of Mo species and meanwhile maintain their high dispersion, however, the enhancement range is limited and the degree is often lower than 80% [21].

More seriously, when using oxidic Mo species as the precursor, another big problem that Ni/Co species are pre-sulfurized into nonactive or lowly-active monometallic sulfides (such as Ni_3S_2 and Co_9S_8) prior to the reduction of oxidic Mo precursors will often be unavoidable [19,28,29], resulting in an inferior decoration of Ni into the edges of MoS_2 phase. To solve this problem, three strategies have been developed, that is, (1) for retarding the pre-sulfidation of Ni/Co, introduce chelating agents (such as NTA, EDTA, citric acid, etc.) into the conventional impregnation liquids to coordinate Ni^{2+}/Co^{2+} ions [30–34], which has been widely applied in the preparation of the industrial hydrotreating catalysts; (2) in order to increase the proximity between Ni/Co and Mo and thereby promote the formation of Ni(Co)-Mo-S phase, use their compounds as the novel precursor, such as $(NH_4)_6Co_2Mo_{10}O_{38}H_4$ [24], $Co_2[Mo_4O_{11}(C_6H_5O_7)]$ [31], etc.; (3) for completely avoiding the pre-sulfidation of Ni/Co prior to Mo and remarkably enhancing the promoting effect, directly introduce some unconventional precursors, such as $Co(CO)_3NO$ [13], $Ni(CO)_4$ [35], Co acetylacetonate [36,37], etc., onto MoS_2 phase by some unfamiliar methods, such as chemical vapor deposition (CVD) and reflux condensation. These strategies have enhanced the promoting effect to an extent, however, there still exit some problems, for instance, the decline of dispersion and stability induced by the introduction of chelating agents [37], the property instability of the CoMo-containing compound during the impregnation process [38,39], the high cost of the Ni/Co precursors and the complexity of their loading methods [26], and so on. It is worthy to note that, all these strategies rely on the basis of using oxidic Mo species as the precursor of MoS_2 phase, and hence, the difficulty to fully sulfurize the Mo species still exists.

To sum up, due to the use of oxidic Mo species as the precursor, the existing preparation technologies and corresponding modification methods could not guarantee the Mo species of the resulting catalysts with well dispersion, full sulfidation and high decoration of Ni/Co at the same time. Many studies on the properties, structure, synthesis and application of MoS_3 species show that [40–44], MoS_3 phase not only possesses flexible micromorphology and microstructure, but also could be transformed into MoS_2 phase via mild thermal treatment. Moreover, the sulfidation process of oxidic Mo species in the conventional hydrotreating catalysts has been generally summarized as $MoO_3 \rightarrow MoO_xS_y \rightarrow MoS_2$ [20], however, some studies have clearly pointed out that, MoS_3 phase is probably another transition state [45–47], further proving the rationality of using MoS_3 nanoparticles (NP_S) as the precursor of active MoS_2 nanoslabs. Herein, by the chemical deposition method reported in the previous studies [48–51], alumina-supported MoS_3 NPs were first synthesized, and then used as the "second support" to load promoter Ni to prepare presulfided NiMo/Al_2O_3 catalysts. The

HDS activities were assessed using the refractory 4,6-dimethyldibenzothiophene (4,6-DMDBT) as the model reactant. To elucidate the superiorities of using MoS_3 as the precursor of active phase, two bimetallic catalysts with the same metal loadings were meanwhile prepared using MoS_2/Al_2O_3 and MoO_3/Al_2O_3 as the starting material, respectively. Results clearly show that, using MoS_3 NPs instead of the conventional oxidic precursors, not only realizes the resulting bimetallic catalyst with a much higher sulfidation degree of Mo species, but also realizes the better decoration of Ni atoms to form more Ni-Mo-S active sites, thus remarkably enhancing the HDS activity.

2. Experimental

2.1. Preparation of pre-sulfided bimetallic NiMo/Al$_2$O$_3$ catalyst

Most high-purity starting materials were purchased from Sinopharm Chemical Reagent Co, Ltd. The pre-sulfided bimetallic catalyst denoted as CAT-MoS$_3$ was prepared through two steps. Firstly, alumina-supported MoS$_3$ NPs denoted as MoS$_3$/Al$_2$O$_3$ were synthesized according to the following procedures: (1) 20 mL of anhydrous ethanol was added into 40 mL of a solution containing 1.02 g of sodium molybdate (Na$_2$MoO$_4$·2H$_2$O) and 1.58 g thioacetamide (CH$_3$CSNH$_2$) under stirring; (2) about 2.4 M HNO$_3$ solution was dropwise added into the above solution to yield an acid solution with pH = 2; (3) the resulting solution was transferred to a 100 mL rotary Teflon-lined stainless steel autoclave containing 4.0 g of γ-Al$_2$O$_3$ extrudates (97.7% Al$_2$O$_3$, average diameter of 1.5 mm, surfaces area of 230 m^2 g^{-1}, pore volume of 0.6 mL g^{-1}, supplied by Sinopec Group) and heated at 85 °C for 10 h; and (4) the resulting solids were filtered, washed and dried at 80 °C in a N$_2$ atmosphere for 5 h to yield MoS$_3$/Al$_2$O$_3$. Secondly, CAT-MoS$_3$ was prepared by the incipient wetness impregnation of MoS$_3$/Al$_2$O$_3$ with an aqueous solution of Ni(NO$_3$)$_2$ with the mole ratio of Ni to Mo at 1:2, followed by drying at 80 °C for 5 h in a N$_2$ atmosphere. The comparative MoO$_3$ and NiO contents in CAT-MoS$_3$ determined by X-ray fluorescence spectroscopy (XRF, Rigaku ZSX-100e) were 8.47 wt.% and 2.18 wt.%, respectively.

For stating the superiorities of using MoS$_3$ as the precursor, two counterpart bimetallic NiMo/Al$_2$O$_3$ catalysts denoted as CAT-MoS$_2$ and CAT-MoO$_3$ with the same Mo and Ni loadings were prepared, respectively. Prior to the preparation of CAT-MoS$_2$, MoS$_2$/Al$_2$O$_3$ was first obtained from the MoS$_3$/Al$_2$O$_3$ composite mentioned above through thermal treatment at 360 °C for 3 h in an atmosphere of H$_2$/Ar (10 vol% H$_2$); and then the Ni atoms were introduced into MoS$_2$/Al$_2$O$_3$ according to the same procedure in the preparation of CAT-MoS$_3$ to prepare CAT-MoS$_2$. Prior to the preparation of CAT-MoO$_3$, MoO$_3$/Al$_2$O$_3$ was first prepared by impregnating γ-Al$_2$O$_3$ with a (NH$_4$)$_6$Mo$_7$O$_{24}$·4H$_2$O solution, followed by drying at 120 °C for 3 h and calcining at 400 °C for 4 h, and then the resulting solid was impregnated by a Ni(NO$_3$)$_2$ solution, dried 120 °C for 3 h and calcined at 400 °C for 4 h to yield CAT-MoO$_3$. Besides, for assessing the promoting effect of CAT-MoS$_3$ and CAT-MoS$_2$, a monometallic MoS$_2$/Al$_2$O$_3$ catalyst was also prepared from the MoS$_3$/Al$_2$O$_3$ through thermal treatment at 360 °C for 3 h under an atmosphere of H$_2$/Ar (10 vol% H$_2$).

2.2. Characterizations

N$_2$ adsorption-desorption measurements were performed on a Micromeritics ASAP 2002 analyzer at liquid nitrogen temperature. Prior to the experiments, the samples were degassed in 250 °C for 15 h under a vacuum of 10^{-5} Torr. The specific surface areas were calculated by the BET method and the pore volumes were calculated from N$_2$ adsorption-desorption isotherms.

X-ray diffraction (XRD) measurements were performed on a Bruker D5005 X'Pert diffractometer equipped with Cu *Kα* radiation (λ = 1.5406 Å). The patterns were collected in the 2θ range between 5° and 70° with a scanning speed of 2° min^{-1}.

X-ray photoelectron spectroscopy (XPS) studies were carried out on a VG Scientific ESCALab250 spectrometer using Al $K\alpha$ radiation. The samples were crushed into powder and kept in a cyclohexane solvent to prevent oxidation. Before measurement, the samples were pressed onto a stainless steel sample holder in air; the holder was immediately moved onto the XPS machine. Quantification of surface content of elements was done using sensitivity factors provided with VG software. Mo species' and Ni species' chemical states (namely Mo^{4+}, Mo^{5+}, Mo^{6+} and Ni-Mo-S, NiO, NiS, Ni shake up) and their contents can be distinguished and quantified by XPS spectrum fitted by XPSPEAK software (Version 4.1).

High-resolution transmission electron microscopic (HRTEM) images of sulfided bimetallic catalysts were taken on a Philips Tecnai G2 F20 instrument, with an electron energy of 220 keV, Cs = 0.5 mm, a point-to-point resolution of 1.9 Å in TEM mode, and a specimen tilt of ± 40°. The images were recorded on a TVIPS 1k × 1k CCD camera. For each catalyst, the average length and stacking of MoS$_2$ nanoslabs were calculated over 500 MoS$_2$ nanoslabs at 30 arbitrary areas. The average slab length ($\overline{L}$), stacking number ($\overline{M}$) and the average fraction of Mo atoms on the edge surface of MoS$_2$ nanoslabs (f_{Mo}) were calculated according to the following two equations [26,52,53], respectively.

$$\overline{L} = \frac{\sum_{i=1}^{n} n_i L_i}{\sum_{i=1}^{n} n_i} \tag{1}$$

$$\overline{M} = \frac{\sum_{i=1}^{m} m_i M_i}{\sum_{i=1}^{m} m_i} \tag{2}$$

$$f_{Mo} = \frac{Mo_{edge}}{Mo_{total}} = \frac{\sum_{i=1}^{n} (6t_i - 6)}{\sum_{i=1}^{n} (3t_i^2 - 3t_i + 1)}. \tag{3}$$

$$t_i = \frac{25L_i}{16} + \frac{1}{2} \tag{4}$$

Where n_i is the number of slabs in a given range of length and L_i is the length of a MoS$_2$ nanoslab; m_i is the number of slabs in a given range of stacks and M_i is the slab stacking layer number; Mo_{edge} and Mo_{total} are the number of Mo atoms located at the edge surface of MoS$_2$ slabs and the total number of Mo atoms of MoS$_2$ slabs, respectively.

2.3. Activity assessment

The catalytic activities of the three bimetallic catalysts and the monometallic MoS$_2$/Al$_2$O$_3$ were assessed in a fixed microreactor with internal diameter of 10.0 mm and length of 500 mm. 0.15 wt% 4,6-DMDBT (provided by J & K Chemical Company) in n-decane was chosen as the model reactant. 0.15 g catalyst to be assessed was diluted with 1.0 mL quartz particles with 0.25 mm in diameter before being loaded into the reactor. Before the HDS test, the three catalysts were all treated with a sulfiding feed of cyclohexane solution containing 5 wt.% CS$_2$ under a H$_2$ pressure of 4.0 MPa and 360 °C for 4 h. The HDS reactions of 4,6-DMDBT were carried out at 280 °C, 300 °C and 320 °C, total pressure 4 MPa, LVSH 58.4 h^{-1}, H$_2$/feed volumetric ratio 500. Then the reaction products were analyzed with Agilent 7890A gas chromatograph. Assuming a psesudo-first-order for 4,6-DMDBT HDS, the HDS reaction activities (denoted as k_{HDS}) of the catalysts were calculated by the following equation [26,53].

$$k_{HDS} = \frac{F_0}{m} \times \ln \frac{1}{1-x} \tag{5}$$

Where F_0 is the feeding rate of reactant 4,6-DMDBT in mol s^{-1}, m is the catalyst mass in g, x is the total conversion of 4,6-DMDBT, and k_{HDS} is the rate constant of 4,6-DMDBT in mol g^{-1} s^{-1}.

Besides, Ni-MoS$_3$ and Ni-MoO$_3$ catalysts with high Mo loadings were also evaluated using a FCC diesel from a Chinese refinery with the sulfur content at ca. 1065 mg L^{-1}. The tests were conducted in a continuously flowing tubular fixed-bed reactor loaded with 4 mL of catalyst diluted with the same volume of quartz particles of diameter 0.25 mm. The HDS assessment was carried out under the following conditions: LHSV 1.5 h^{-1}, temperature 360 °C, total pressure 6.0 MPa, and H$_2$/oil volume ratio 500.

3. Results and discussion

3.1. Characterization results of alumina-supported MoS$_3$ NPs

3.1.1. XPS

XPS analysis was first carried out to demonstrate the chemical state of the Mo species supported on alumina, and the Mo3d and S2p spectra are shown in Fig. 1a and b, respectively. According to the surface element analysis results, the S/Mo atomic ratio is about 2.90, which is very closely to the standard stoichiometric number of MoS$_3$. Considering the fact that Mo species maybe present as well-dispersed particles with nanoscale size on alumina surface, the slightly lower value than 3 is reasonable [54]. For further assuring the species are ascribed to MoS$_3$, the curves of Mo3d and S2p were fitted, as shown in Fig. 1a and b, respectively. The Mo 3d region reveals a mixture of Mo oxidation states, and peak fitting illustrates that ~23.8% of the Mo signal belongs to the Mo^{6+} and ~76.2% of Mo signal arises from the molybdenum sulfide, which likely belongs to the lower oxidation state of Mo^{4+} [55]. The curve-fitted S2p spectra consist of two doublets with S2p$_{3/2}$ energies of
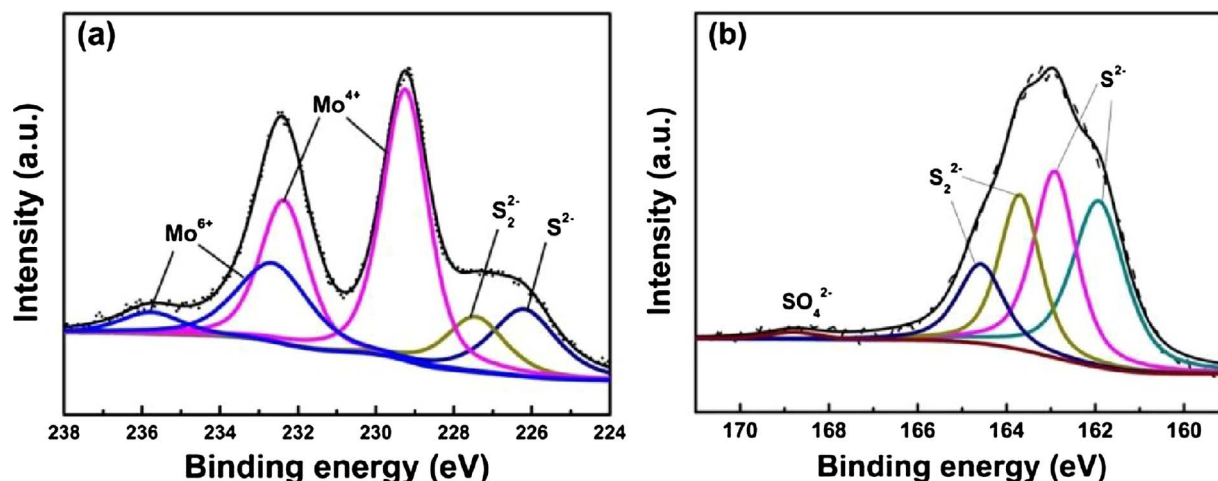

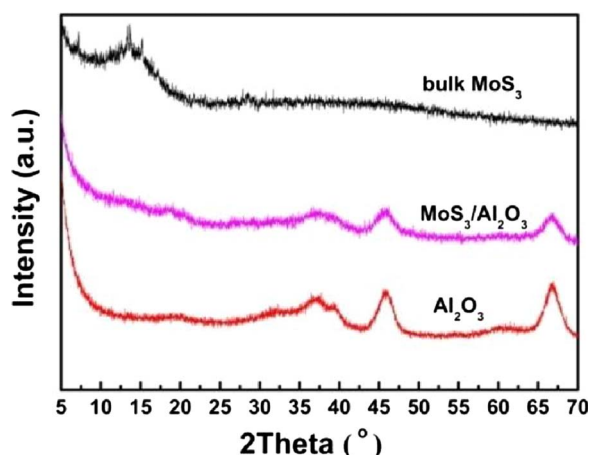Fig. 1. XPS spectra of the measured and curve-fitted Mo3d orbits (a) and S2p orbits (b) of MoS$_3$/Al$_2$O$_3$ composite.

Fig. 2. XRD patterns of γ-Al₂O₃, MoS₃/Al₂O₃ and bulk MoS₃.

Fig. 4. N₂ adsorption-desorption isotherms (a) and pore size distribution curves (b) of γ-Al₂O₃ and MoS₃/Al₂O₃.

162.0 eV and 163.3 eV ascribed to S^{2-} and S_2^{2-} ligands, respectively, which is one characteristic of MoS_3 [42–44]. Furthermore, the relative intensity of the two doublets is about 5:4, which is very consistent with the previous reports on amorphous MoS_3 materials [55,56]. In summary, the synthesized Mo species supported on alumina can be ascribed as amorphous MoS_3. Besides, a small peak observed near 169.0 eV is ascribed to the S2p spectrum of SO_4^{2-}, which is probably yielded in the chemical-deposition process[50].

3.1.2. XRD

XRD measurements were conducted to understand the distribution state of MoS_3 particles on the alumina surface, and the XRD patterns of MoS_3/Al_2O_3 and γ-Al_2O_3 are shown Fig. 2. For comparison purpose, the pure MoS_3 material was meanwhile analyzed and the results are also shown in Fig. 2. The peak at about 14.2° is ascribed to the amorphous bulk MoS_3 and the peaks at 37.3°, 45.9° and 66.7° are attributed to γ-Al_2O_3 [25,26]. It is clearly shown that, MoS_3/Al_2O_3 exhibits only characteristic peaks of γ-Al_2O_3, powerfully indicating MoS_3 particles supported on alumina surface are too small to be detected by XRD [57]. Considering that the detectability of XRD analysis is about 4 nm [26], the above results imply that most MoS_3 particles in MoS_3/Al_2O_3 are well dispersed on γ-alumina surface with a nanosize smaller than 4 nm.

3.1.3. HRTEM

To further confirm the alumina supported MoS_3 particles with the nanoscale size, the HRTEM images of $MoS_3/γ-Al_2O_3$ were taken, and the typical image is shown in Fig. 3a. Due to the same amorphous state of MoS_3 particles and alumina surface [43,44], it is difficult to distinguish them from each other, and hence it is unable to observe the microstructure and micromorphology of the MoS_3 particles in Fig. 3a. However, due to the in-situ thermal decomposition from MoS_3 to MoS_2, the microscopic dimensions of MoS_3 particles can be indirectly reflected by the derivedMoS_2 particles. So the HRTEM images of monometallic $MoS_2/γ-Al_2O_3$ catalyst originated from $MoS_3/γ-Al_2O_3$ composite were
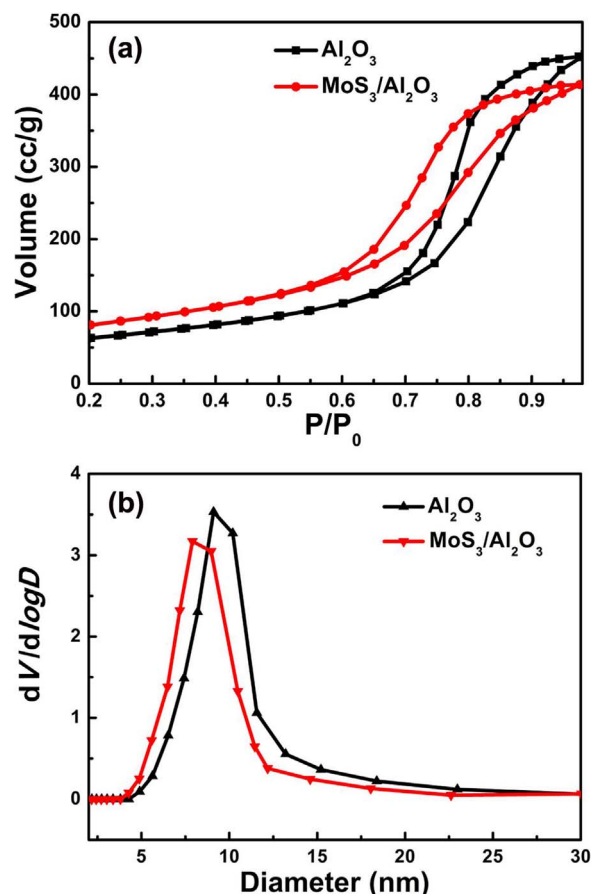
also taken, and the typical image is shown in Fig. 3b. It clearly shows that, $MoS_2/γ-Al_2O_3$ contains many well-dispersed lamellar crystallites (as indicated by white arrows) with majority of the size lower than 4 nm. It is not difficult by the EDX analysis to ascribe the crystallites as MoS_2 nanoslabs [50]. Hence, the HRTEM images of $MoS_2/γ-Al_2O_3$ powerfully indicate that its precursor $MoS_3/γ-Al_2O_3$ is certainly constructed by numerous well-dispersed MoS_3 NPs supported on alumina surface, which is consistent with the above XRD analysis results.

3.1.4. N₂ adsorption-desorption

The N₂ adsorption-desorption isotherms of γ-Al_2O_3 and MoS_3/Al_2O_3 are shown in Fig. 4a, which are both type IV ones with a typical H2 type hysteresis loop, indicating they hold typical mesoporous structure. Their pore size distributions are shown in Fig. 4b, which clearly shows that, compared with that of γ-Al_2O_3, the pore size distribution of the MoS_3/Al_2O_3 composite becomes narrower and the most probable pore diameter decreases greatly from ca. 9.5 nm to ca. 8.0 nm. The textural
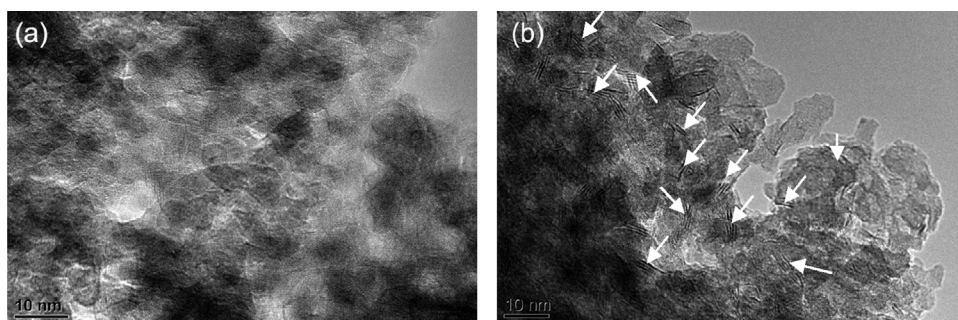

Fig. 3. Typical HRTEM images of the MoS₃/γ-Al₂O₃ composite with a amorphous surface (a) and its derived monometallic MoS₂/Al₂O₃ catalyst with well-dispersed MoS₂ nanoslabs as indicated by the white arrows (b).

Table 1

XRF and N_2 adsoption-desorption analysis results of γ-Al_2O_3, MoS_3/Al_2O_3 and the three bimetallic catalysts prepared using different Mo species as the precursor.

Samples	XRF analysis results		Textual properties		
	MoO_3,wt%	NiO,wt%	$S_g{}^a$, $m^2\,g^{-1}$	$V_p{}^b$, $cm^3\,g^{-1}$	$D_p{}^c$, nm
γ-Al_2O_3	–	–	230	0.79	9.2
MoS_3/Al_2O_3	8.51	–	219	0.66	7.9
CAT-MoS_3	8.47	2.18	218	0.69	7.9
CAT-MoS_2	8.47	2.22	213	0.68	8.0
CAT-MoO_3	8.48	2.21	215	0.67	8.0

Notes: [a]BET surface area; [b]Pore volume; [c]Average pore diameter.

properties of MoS_3/Al_2O_3 and γ-Al_2O_3 are shown in Table 1. It clearly shows that, compared with γ-Al_2O_3, the specific surface area (from 230 to 219 $m^2\,g^{-1}$), pore volume (from 0.79 to 0.66 $mL\,g^{-1}$), and average pore diameter (from 9.2 to 7.9 nm) of MoS_3/Al_2O_3 all undergo obvious decline, further indicating that MoS_3 NPs are well-dispersed on the internal/external surface of the pores of γ-Al_2O_3 [25,26,50].

3.2. Characterization results of the bimetallic NiMo/Al_2O_3 catalysts

3.2.1. XRF, N_2 adsorption-desorption and XRD

The metal loadings and textural properties of MoS_3/Al_2O_3-derived bimetallic NiMo/Al_2O_3 catalyst CAT-MoS_3 and its two counterparts CAT-MoS_2 and CAT-MoO_3 are shown in Table 1. Fig. 5a and b show the N_2 adsorption-desorption isotherms and the pore size distributions of the three catalysts, respectively. By combination of Table 1 and Fig. 5, it can be concluded that, the three bimetallic catalysts possess very similar metal loadings and textural properties.
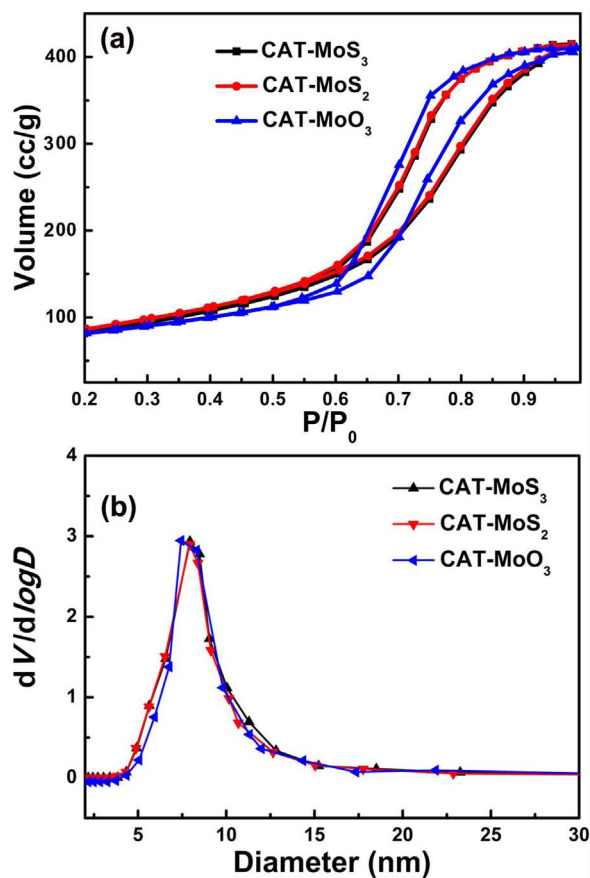

Fig. 5. N_2 adsorption-desorption isotherms (a) and pore size distribution curves (b) of the three bimetallic catalysts.
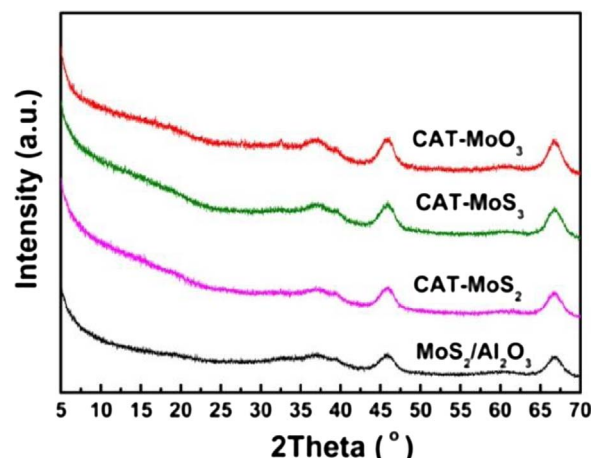

Fig. 6. XRD patterns of the three bimetallic catalysts and the one monometallic MoS_2/Al_2O_3 catalyst.

Fig. 6 shows the XRD patterns of the three bimetallic catalysts and the monometallic MoS_2/Al_2O_3 catalyst. It can be clearly seen that, except of the characteristic peaks of γ-Al_2O_3 at 37.2°, 45.6° and 66.9° [25,26], there are no signals of Mo species or Ni species. The results indicates that the Mo species in the four catalyst are most probably amorphous and well-dispersed on the alumina surface, and the absence of nickel peak may be due to the low concentration which is below the XRD detection limit.

The above results imply that the three bimetallic catalysts exhibit a similar composition and physical properties, thus laying a foundation of studying the fundamental advantages of using MoS_3 NPs instead of MoS_2 or MoO_3 NPs as the precursor to prepare bimetallic NiMo/Al_2O_3 catalysts.

3.2.2. HRTEM

The representative HRTEM micrographs of the three sulfided bimetallic catalysts are shown in Fig. 7a–c, respectively. The statistical results of the length and stacking number distributions of MoS_2 slabs are displayed in Fig. 8a and b, respectively. The average lengths and average stacking numbers over the three bimetallic catalysts are also calculated according to the equations mentioned in Section 2.2, as listed in Table 2. In some studies [15,26], the fraction of Mo atoms on the edge surface of the MoS_2 slabs (f_{Mo}) are adopted to indicate the dispersion state of the active phase. Herein, the f_{Mo} values of the three catalysts are also listed in Table 2. The statistical results (Fig. 8), as well as the HRTEM micrographs of the sulfided CAT-MoS_3 and CAT-MoS_2 show that they possess very similar distribution and micromorphology of MoS_2 nanoslabs, as further confirmed by their very close average length (3.30 nm *vs.* 3.33 nm), average stacking layer number (3.4 *vs.* 3.2) and f_{Mo} (0.31 *vs.* 0.31). It is not difficult to explain the comparability, that is, the two catalysts both originated from the same precursor, i.e., MoS_3/Al_2O_3. The results are very important, and it will help to directly ascribe the activity difference of the two catalysts to their different Ni-decoration onto the edges of MoS_2 nanoslabs. As different to CAT-MoS_3 and CAT-MoS_2 which both originated from MoS_3/Al_2O_3, MoO_3/Al_2O_3-derived CAT-MoO_3 possesses much narrower stacking number distribution (Fig. 8a) and wider layer length distribution (Fig. 8b), which is further demonstrated by its MoS_2 slabs with a much lower average stacking number, a higher average length and a lower fraction of Mo_{edge} (f_{Mo} = 0.29), as listed in Table 2. Many studies have pointed out that, a highly active HDS catalyst should be composed of type II active sites as many as possible [13,22,26,35,36], which means each MoS_2 slab should exhibit a lower length, a higher stacking and a larger f_{Mo}. Based on this viewpoint, the above HRTEM results indicate that, by using MoS_3 NPs instead of the conventional MoO_3 NPs as the precursor one can obtain a series of catalysts with a better microstructure.
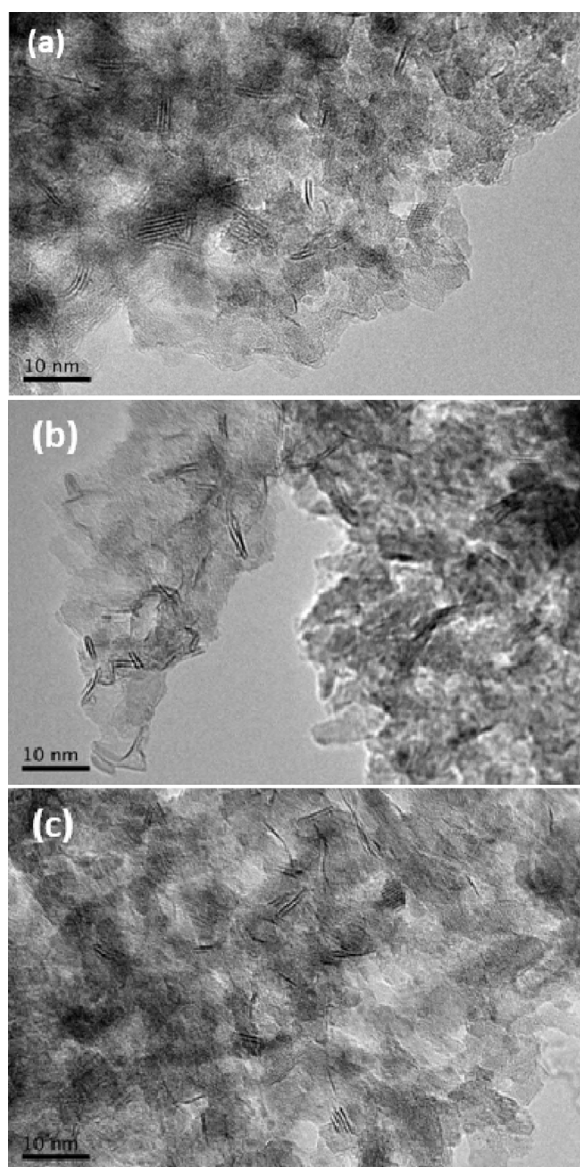
Fig. 7. Typical HRTEM images of the three bimetallic catalysts prepared using different Mo species as the precursor: CAT-MoS₃ (a), CAT-MoS₂ (b), and CAT-MoO₃ (c).
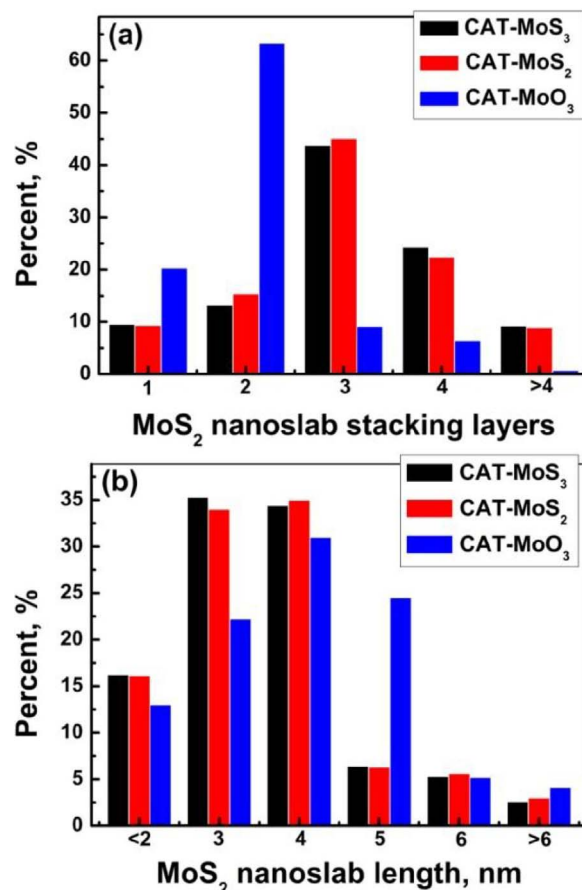

Fig. 8. Distributions of the lengths (a) and layer numbers (b) of MoS₂ nanoslabs on the three bimetallic catalysts prepared using different Mo species as the precursor.

Table 2
HRTEM characterization results of the three bimetallic catalysts prepared using different Mo species as the precursor.

Catalysts	Average length, nm	Average stacking number	f_{Mo}
CAT-MoS₃	3.30	3.4	0.31
CAT-MoS₂	3.33	3.2	0.31
CAT-MoO₃	3.59	2.1	0.29

3.2.3. XPS

For an insight into the chemical state of Mo species and Ni species, the Mo3d and Ni2p spectra together with their corresponding deconvoluted curves of CAT-MoS₃, CAT-MoS₂ and CAT-MoO₃ are displayed in Fig. 9a–f, respectively. The binding energies of the Mo3d$_{5/2}$ and Mo3d$_{3/2}$ peaks for Mo^{4+} (MoS₂) appear at about 229.0 and 232.1 eV, while those for Mo^{6+} (MoO₃) appear at about 232.5 and 235.7 eV, and that of the S2s peak appears at about 226.2 eV [58]. The binding energy of the Ni2p peak for Ni-Mo-S active phase appear at about 854.1 eV, while those for Ni sulfides (NiS$_x$) appear at about 853.2 eV, and that for oxidic Ni^{2+} species (i.e., NiO$_x$, including NiAl₂O₄ and NiO) appears at about 856.7 eV [58]. Besides, the peak in Ni2p spectra in about 862.5 eV is ascribed to the shake up of the oxidic Ni^{2+} species [58]. It can be clearly seen that, obviously different from the Mo3d spectra of CAT-MoO₃ showing characteristics of the MoS₂, MoO$_x$S$_y$ and MoO₃ species, those of CAT-MoS₃ and CAT-MoS₂ exhibit almost the same curves with predominant characteristic peaks of the MoS₂ species and weak characteristic peaks of the MoO₃ species. However, the Ni2p spectra of the three bimetallic catalysts show the same characteristics of Ni-Mo-S phase, oxidic Ni^{2+} species. It is noteworthy that, the characteristic peak

ascribed to NiS$_x$ was not found in this research, probably due to the much lower metal loadings in the three catalysts than in the industrial hydrotreating catalysts.

For further quantizing distribution of Mo species and Ni species, the sulfidation degree of Mo species (denoted as Mo_{sul}) and the decoration degree of Ni species onto edges of MoS₂ nanoslabs (denoted as Ni$_{NiMoS}$/Ni$_{total}$) were calculated according to the following methods [59,60]. For Mo_{sul}, it is defined as the ratio of Mo^{4+} (MoS₂) to the sum of Mo^{4+} (MoS₂), Mo^{5+} (Mo$_x$S$_y$), and Mo^{6+} (MoO₃), i.e., Mo_{sul} = Mo^{4+}/(Mo^{4+} + Mo^{5+} + Mo^{6+}). For Ni$_{NiMoS}$/Ni$_{total}$, it is equal to the molar ratio of Ni^{2+} in Ni-Mo-S phase (denoted as Ni$_{NiMoS}$) to the sum of Ni$_{NiMoS}$, Ni^{2+} in NiS$_x$ phase (denoted as Ni$_{NiSx}$), and oxidic Ni^{2+} (denoted as Ni$_{NiOx}$), i.e., Ni$_{NiMoS}$/Ni$_{total}$ = Ni$_{NiMoS}$/(Ni$_{NiMoS}$ + Ni$_{NiSx}$ + Ni$_{NiOx}$). The Mo_{sul} and Ni$_{NiMoS}$/Ni$_{total}$ of the three catalysts are shown in Table 3. It can be seen that, the Mo_{sul} of CAT-MoS₃ and CAT-MoS₂ catalysts both reach up to above 94%, which are largely higher than that of CAT-MoO₃ (only 69.8%), indicating that using MoS₃ instead of the traditional MoO₃ as active phase precursor could significantly improve the sulfidation degree of Mo species. Although CAT-MoS₃ and CAT-MoS₂ hold the similar Mo_{sul}, the Ni$_{NiMoS}$/Ni$_{total}$ value (45.6%) of the former is much larger than that (30.7%) of the latter,
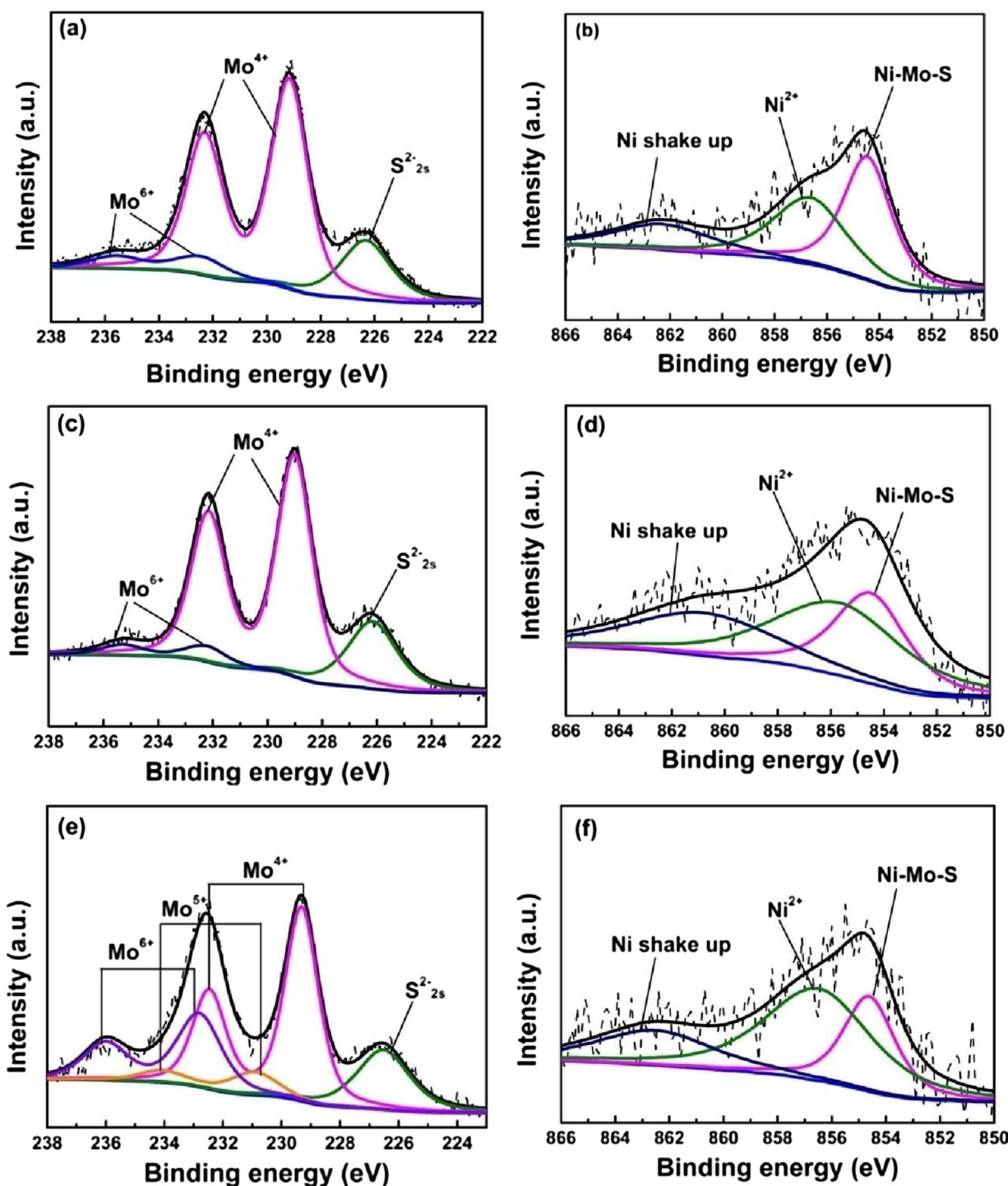
Fig. 9. XPS survey spectra of the measured and curve-fitted Mo 3d and Ni 2p orbits of CAT-MoS$_3$ (a) and (b); CAT-MoS$_2$ (c) and (d); and CAT-MoO$_3$ (e) and (f), respectively.

Table 3
Mo_{sul} and Ni$_{NiMoS}$/Ni$_{total}$ of the three bimetallic catalysts prepared using different Mo species as the precursor.

Catalysts	Mo_{sul}, %	Ni$_{NiMoS}$/Ni$_{total}$, %
CAT-MoS$_3$	94.2	45.6
CAT-MoS$_2$	94.3	30.7
CAT-MoO$_3$	69.8	36.9

powerfully demonstrating that the starting state of the Mo species imposes an essential effect on the decoration of Ni species onto the edges of MoS$_2$ nanoslabs. Very interestingly, although CAT-MoO$_3$ holds a much lower Mo_{sul} than CAT-MoO$_3$ (69.8% vs. 94.3%), it still exhibits an obviously higher Ni$_{NiMoS}$/Ni$_{total}$ (36.9% vs. 30.7%), further indicating that the Ni-decoration degree is greatly influenced by the type of Mo species. Moreover, the obvious larger Ni$_{NiMoS}$/Ni$_{total}$ (45.6%) of CAT-MoS$_3$ than that of CAT-MoO$_3$ (36.9%) implies that, except for remarkably enhancing the Mo_{sul}, using MoS$_3$ NPs as the precursor could also greatly improve the Ni-decoration degree to maximize the formation of type II Ni-Mo-S active sites.
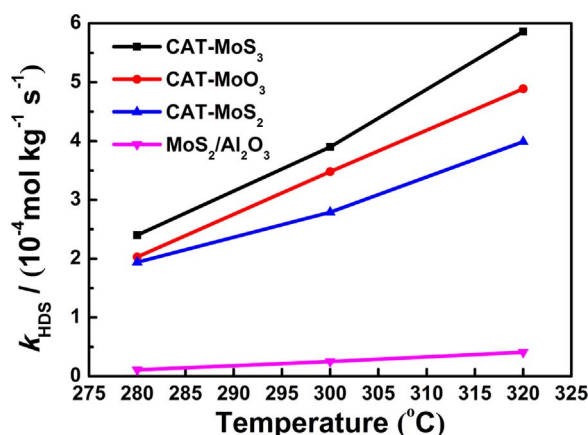
Fig. 10. HDS activities of the three bimetallic catalysts and the one monometallic MoS_2/Al_2O_3 catalyst.

Fig. 11. HDS reaction network of 4,6-DMDBT.

3.3. HDS activities of the bimetallic NiMo/Al₂O₃ catalysts

4,6-DMDBT has been widely considered as the most refractory sulfur-containing compound in transportation fuels [57,61], and herein it was chosen as the model reactant to evaluate the performance of HDS catalysts in this study. The HDS activities of the three bimetallic catalysts and the monometallic catalyst MoS_2/Al_2O_3 as a function of temperature are shown in Fig. 10. It is clearly seen that, regardless of the reaction temperature, the HDS activity of the three bimetallic catalysts follow the clear-cut order of CAT-MoS₃ > CAT-MoO₃ > CAT-MoS₂. Moreover, with the reaction temperature increasing from 280 °C to 320 °C, their activity increment follows the same order, which means that the more active catalyst, the more temperature-sensitive and the more obvious performance advantages. Besides, the nearly ignored HDS activity of the monometallic MoS_2/Al_2O_3 as compared with the three bimetallic catalysts fully demonstrates that a well promoting effect is vital for a highly-efficient HDS catalyst [9,13–15,26,35,36,50]. In order to further compare the activities of the four catalysts, their HDS activities at 320 °C, 4 MPa are listed in Table 4. It shows that, the k_{HDS} of CAT-MoS₃ is 3.90×10^{-4} mol kg^{-1} s^{-1}, larger than that (3.44×10^{-4} mol kg^{-1} s^{-1}) of CAT-MoO₃, and much larger than that (2.66×10^{-4} mol kg^{-1} s^{-1}) of CAT-MoS₂. Specially, the k_{HDS} of the monometallic catalyst MoS_2/Al_2O_3 is 0.25×10^{-4} mol kg^{-1} s^{-1}, only several tenths of the three bimetallic catalysts. Furthermore, due to the origination of the same precursor MoS_3/Al_2O_3, the Ni-promoting effect for CAT-MoS₃ and CAT-MoS₂ were compared through the synergetic factor, which is defined by dividing k_{HDS} (Ni-MoS₂/Al₂O₃) by k_{HDS} (MoS₂/Al₂O₃) [26]. The synergetic factor for CAT-MoS₃ is 15.60, while that for CAT-MoS₂ is only 10.64, indicating that MoS₃ NPs can function as an excellent "second support" for Ni atoms [13,26], and whereas using MoS₂ NPs as the second support isnot helpful to enhance the promoting effect.

The HDS reaction networks of 4,6-DMDBT is proposed as shown in Fig. 11 [57,61,62]. For 4,6-DMDBT HDS, it mainly proceeds through two pathways: one is direct desulfurization (DDS) route to produce 3,3′-
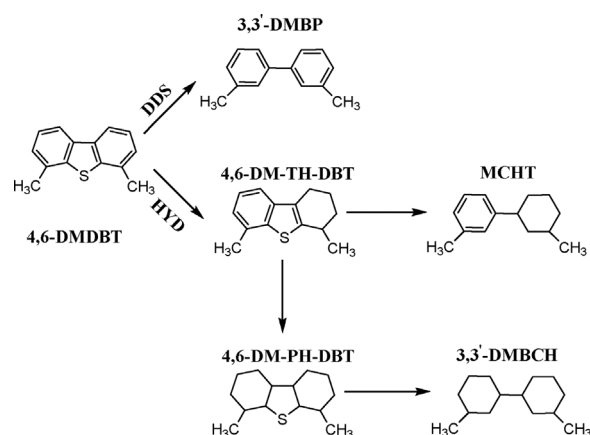
DMBP, and another is through the hydrogenation (HYD) route to obtained MCHT and 3,3′-DMBCH, 4,6-DM-TH-DBT and 4,6-DM-PH-DBT as the intermediates. Hence, the reaction rate constants for the DDS route (k_{DDS}) and the HYD route (k_{HYD}) are expressed by the following two equations [62], respectively.

$$k_{DDS} = K_{HDS} \times S_{BP} \tag{6}$$

$$k_{HYD} = K_{HDS} \times S_{MCHT + 3,3'-DMBCH} \tag{7}$$

Where S_{BP} and $S_{MCHT+3,3'-DMBCH}$ represent the selectivity to the different HDS products of routes DDS and HYD, respectively, ant their sum is equal to the total HDS activity, noted as k_{HDS}. K_{HDS} means the total reaction rate, involving desulfurization reactions and the intermediate reactions.

The selectivity results of the two reaction routes over the three bimetallic catalysts and the one monometallic catalyst are also listed in Table 4. As confirmed by the k_{HYD}/k_{DDS} values of the four catalysts from 4.0 to 5.3 in Table 4, their 4,6-DMDBT HDS reactions mainly proceed through HYD route, which can be attributed to the steric hindrance effect of 4,6-DMDBT on the DDS route [61]. However, compared with CAT-MoO₃ and CAT-MoS₂, CAT-MoS₃ exhibit much higher k_{HYD} and k_{DDS}. Very interestingly, k_{HYD}/k_{DDS} and k_{HDS} follow the same order of CAT-MoS₃ > CAT-MoO₃ > CAT-MoS₂, indicating that the enhanced HDS activity of CAT-MoS₃ as compared to CAT-MoO₃ and CAT-MoS₂ mainly contributed by the increase of HYD activity. This result is different from the previous study [50], in which DBT with no steric hindrance was chosen as the model reactant.

The above results showed that, using MoS_3/Al_2O_3 as the precursor has realized the resulting catalyst CAT-MoS₃ with a remarkable enhancement of HDS activity. However, the metal loadings (i.e., comparable MoO₃ 8.47 wt.% and NiO 2.18 wt.%) are much lower than those in industrial HDS catalysts. Herein, in order to investigate the industrial application potential, a CAT-MoS₃ with comparable MoO₃ 15.03 wt.% and NiO 3.41 wt.% (denoted as CAT-MoS₃-15) was prepared according to the following steps: first impregnate γ-Al₂O₃ with an aqueous solution of MoS_4^{2-} (its novel synthesis method will be

Table 4
HDS results over the three bimetallic catalysts and the one monometallic MoS_2/Al_2O_3 catalyst at 300 °C, 4 MPa.

Catalyst	k_{HDS} (10^{-4} mol kg^{-1} s^{-1})	SF_{HDS}	k_{HYD} (10^{-4} mol kg^{-1} s^{-1})	k_{DDS} (10^{-4} mol kg^{-1} s^{-1})	k_{HYD}/k_{DDS}
CAT-MoS₃	3.90	15.60	3.28	0.62	5.3
CAT-MoS₂	2.66	10.64	2.19	0.47	4.7
CAT-MoO₃	3.48	–	2.91	0.57	5.1
MoS₂/Al₂O₃	0.25	–	0.20	0.05	4.0

Notes: k_{HDS} are the total desulfurizationreaction rate constant 4,6-DMDBT; SF_{HDS} is the synergetic factor, which is equal to k_{HDS}(Ni-MoS₂/Al₂O₃)/k_{HDS}(MoS₂/Al₂O₃); k_{HYD} and k_{DDS} represent the desulfurization activity HYD (hydrogenation) path and DDS (direct desulfurization) path, respectively; for rationally analyzing the reactive selectivity, the conversions were controlled nearly the sameby modifying the feeding rate when needed.
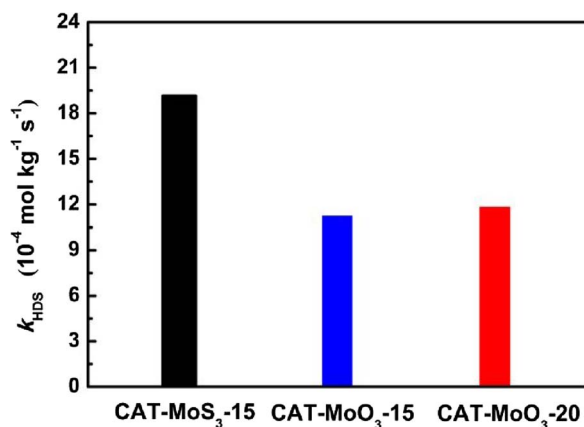
Fig. 12. HDS activity of Ni-MoS$_3$ and Ni-MoO$_3$ catalysts with high Mo loadings under the reaction conditions of 320 °C and 4 MPa.
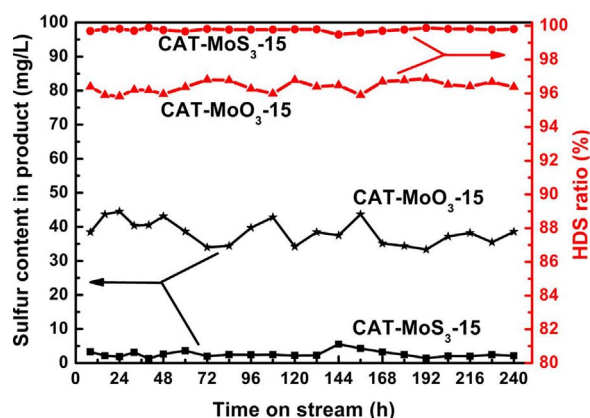

Fig. 13. Sulfur content in the diesel products (Left) and HDS ratio (Right) with time on stream over CAT-MoS$_3$-15 and CAT-MoO$_3$-15.

reported in the near future), followed by a thermal treatment at about 200 °C under an atmosphere of H$_2$ [47,63,64], to obtain a MoS$_3$/Al$_2$O$_3$ composite, and then introduce the Ni atoms into the composite by impregnation method, followed by the subsequent procedures described in Section 2.1 to fabricate CAT-MoS$_3$-15. For comparison purpose, two conventional CAT-MoO$_3$ catalysts denoted as CAT-MoO$_3$-15 and CAT-MoO$_3$-20 with MoO$_3$ 15.0 wt.% and MoO$_3$ 20.0 wt.%, respectively, were prepared according to the methods as used to prepare CAT-MoO$_3$ described in Section 2.1. The HDS activities of CAT-MoS$_3$-15, CAT-MoO$_3$-15 and CAT-MoO$_3$-20 are shown in Fig. 12, It clearly shows that, the HDS activity of CAT-MoS$_3$-15 is not only nearly two times higher than that of CAT-MoO$_3$-15 which contains the same metal loadings, but also even 1.6 times higher than that of CAT-MoO$_3$-20 which possesses higher metal loadings. Moreover, under the experimental conditions, the HDS ratio of CAT-MoS$_3$-15 could reach up to 100%. Besides, the HDS activity of catalysts CAT-MoS$_3$-15 and CAT-MoO$_3$-15 were also assessed using the real FCC diesel as feedstock and the results are shown in Fig. 13. During the operation for 240 h, the sulfur content in the product obtained over the two catalysts remained stable, with the HDS ratio obtained over CAT-MoS$_3$-15 being obviously higher than that over CAT-MoO$_3$-15, revealing the remarkably enhanced HDS activity of CAT-MoS$_3$-15. The above results imply that, using MoS$_3$ NPs as the novel precursor holds a great potential for industrial applications.

3.4. Enhancement origin of promoting effect using MoS$_3$ as the precursor of MoS$_2$

According to the characterization and activity assessment results

above, the orders of the sulfidation degrees of Mo species, the Ni-decoration degrees and the HDS activities of the three bimetallic catalysts can be summarized as follows, respectively, that is CAT-MoS$_3$ ≈ CAT-MoS$_2$ > CAT-MoO$_3$,   CAT-MoS$_3$ > CAT-MoO$_3$ > CAT-MoS$_2$ and CAT-MoS$_3$ > CAT-MoO$_3$ > CAT-MoS$_2$. Thereinto, in comparison with CAT-MoS$_2$, CAT-MoS$_3$ possesses the similar physical properties, microstructure and sulfidation degree of Mo species, but exhibits much higher HDS activity, only because of its much higher Ni-decoration degree. Compared with CAT-MoS$_2$, CAT-MoO$_3$ exhibits a worse microstructure and much lower sulfidation degree of Mo species, whereas due to its larger Ni-decoration degree, it still exhibits a more excellent HDS activity. These results clearly indicate that the starting state of the Mo species has a direct and great influence on the catalytic performance. Furthermore, compared with the sulfidation degree of Mo species, the Ni-decoration degree of Ni atoms onto the edges of MoS$_2$ nanoslabs imposes a more important influence on the catalytic performance. In other words, the improvement of HDS performance induced by using MoS$_3$ NPs as the precursor is mainly contributed by the enhancement of the Ni-decoration degree.

Although many researches have studied the amorphous MoS$_3$ material by virtue of a variety of physical and chemical techniques, together with theoretical calculation methods [47,55,65–67], no consensus about its microstructure has yet been reached. It seems the chain structure has been widely recognized, and based on this structure, two models were suggested [65]: (1) Mo^{IV}(S$_2$$^{2-}$)(S^{2-}), there are bridging disulfides between each pair of molybdenum atoms; (2) Mo^{V}(S$_2$$^{2-}$)$_2$(S$_2$$^{2-}$)$_{1/2}$, there are disulfide groups bridging the Mo-Mo bonded pairs. According to XPS analysis in this study, two oxidation states (Mo^{4+} and Mo^{6+}) exist in Mo species of MoS$_3$/Al$_2$O$_3$, which are different from the above two models, but consistent with some other studies [43,44,55]. However, there are indeed two chemical states of sulfur, i.e., S^{2-} and S$_2$$^{2-}$, in MoS$_3$/Al$_2O_3$. Nevertheless, it has been established that the thermal decomposition of amorphous MoS$_3$ will result in a poorly crystalline of MoS$_2$ [47,63,64,67]. Especially, under an atmosphere of H$_2$, the thermal stability of MoS$_3$ will be decreased and the decomposition will be promoted [63,64]. Further studies on the decomposition of MoS$_3$ into MoS$_2$ suggested that [6,68–70], the process involves a dynamical structure reconstruction, in which the Mo-S and Mo-S$_2$$^{2-}$ bonds are broken into new Mo-S bonds to rebuild a new structure of MoS$_2$ with abundant lattice-defect sites.

Based on these research conclusions, the enhancement mechanism of promoting effect through using MoS$_3$ NPs as the precursor can be suggested as illustrated by Fig. 14a: when the promoter Ni species are introduced into the MoS$_3$/Al$_2$O$_3$ composite, followed by thermal treatment at 360 °C under a H$_2$/H$_2$S atmosphere, the MoS$_3$ NPs will undergo the dynamical structure reconstruction mentioned above to form MoS$_2$ structure with plenty of lattice-defect sites, and the Ni^{2+} adsorbed on MoS$_3$ NPs will thereupon occupy the defect sites to form Ni-Mo-S active sites. On the contrary, when using MoS$_2$ NPs as the precursor (Fig. 14b), the dynamical structure reconstruction is probably absent, and it is thereby difficult to yield additional defect sites to accommodate the adjacent Ni^{2+} to form more Ni-Mo-S active sites, thus resulting in a non-ideal promoting effect. However, when using conventional MoO$_3$ NPs as the precursor (Fig. 14c), although the oxidic Mo species could not attain a full sulfidation (only 69.8%) due to the strong metal-support interaction, CAT-MoO$_3$ still exhibits a much higher promoting effect than CAT-MoS$_2$ which holds nearly-full sulfidation degree of Mo species (94.3%). It is not difficult to explain that, the transformation from MoO$_3$ to MoS$_2$ involves a series of fine structure evolutions, e.g. MoO$_3$ → MoO$_x$S$_y$ → MoS$_3$ → Mo$_{2+x}$ → … → MoS$_2$ → MoS$_{2-x}$, as suggested by many studies, and it is actually accompanied by the formation and growth of MoS$_2$ crystallites, which is beneficial to the formation of defect sites to accommodate the Ni^{2+} to produce Ni-Mo-S active sites. Moreover, considering that the strong metal-support interaction and the resulting low sulfidation degree of Mo species, it can be explained that why the Ni-decoration degree of CAT-MoO$_3$ is smaller
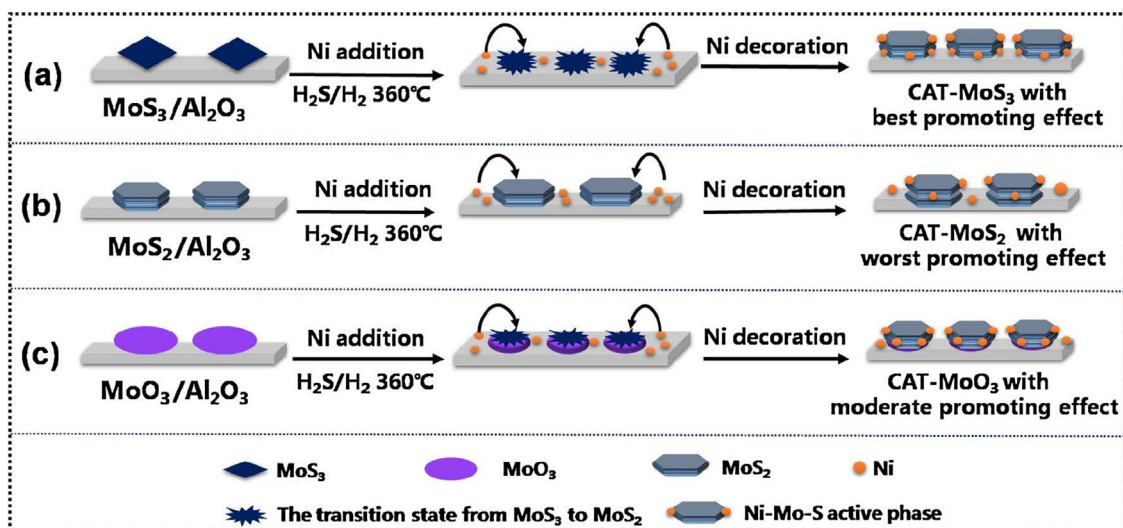
Fig. 14. Schematic diagram of enhancement mechanism of promoting effect through using MoS$_3$ NPs as the precursor.

than that of CAT-MoS$_3$, as shown in Fig. 14a and c.

In addition, it is noteworthy that, by virtue of some unconventional technologies, such as CVD and reflux condensation, some studies introduced the promoter atoms (Ni or Co) onto the as-prepared monometallic MoS$_2$/Al$_2$O$_3$ catalysts and found that the promoting effects attained great enhancement [13,35,36]. However, it is not found in CAT-MoS$_2$ prepared through introducing Ni atoms into MoS$_2$/Al$_2$O$_3$ by the conventional impregnation method in this study, and the promoting effects is the worst in the three bimetallic catalysts. These studies ascribed the enhancement of decoration degree to the strengthened proximity between Ni/Co atoms and MoS$_2$ induced by the novel physical technologies. However, considering that the dynamical structure reconstruction maybe the requirement for an ideal decorationdegree discussed above, the increasing structural instability of MoS$_2$ nanoslabs brought by the powerful energy of the novel physical techniques is probably the essential reason for the improvement of the promoting effect. Hence, except for modifying the starting state of Mo species to improve the promoting effect by, developing novel introduction technologies of promoter atoms is probably another effective strategy.

4. Conclusions

In summary, γ-alumina-supported MoS$_3$ NPs synthesized by chemical deposition method were first used as the starting material to prepare a bimetallic NiMo/Al$_2$O$_3$ catalyst CAT-MoS$_3$. Meanwhile, CAT-MoS$_2$ and CAT-MoO$_3$ with the same metal loadings were prepared through using MoS$_2$/Al$_2$O$_3$ and MoO$_3$/Al$_2$O$_3$ as the starting material, respectively. Characterization and HDS activity assessment results show that, using MoS$_3$ as a novel precursor exhibit two obvious advantages: (1) promotes the resulting bimetallic catalyst with a much higher sulfidation degree of Mo species (reach up to above 94%); (2) realizes the better decoration of Ni atoms onto the edges of MoS$_2$ nanoslabs to form more Ni-Mo-S active sites. The dual effect guarantees the formation of Type II Ni-Mo-S active sites and thus remarkably enhances the HDS activity.

Furthermore, through comparatively deducing the structure-function relations of CAT-MoS$_3$ *vs.* CAT-MoS$_2$, and CAT-MoO$_3$ *vs.* CAT-MoS$_2$, respectively, it was concluded that the HDS activity improvement induced by using MoS$_3$ NPs as the precursor should be mainly contributed by its role in enhancing the Ni-decoration degree. And the enhancement origin of promoting effect using MoS$_3$ as the precursor was suggested as follows: MoS$_3$ structure is very thermally unstable, when treated by a suitable temperature under an atmosphere of H$_2$, it will undergo a dynamical structure reconstruction to form MoS$_2$

structure with abundant lattice-defect sites on the edge surface, which facilitates to accommodate promoter atoms to form more Ni-Mo-S active sites.

The success of this work provides a novel precursor for preparing supported metal sulfide catalysts and indicates that modifying the starting state of Mo species to improve the promoting effect is an effective way to enhance the performance of the catalysts.

References

[1] C. Song, An overview of new approaches to deep desulfurization for ultra-clean gasoline, diesel fuel and jet fuel, Catal. Today 86 (2003) 211–263.

[2] A. Pimerzin, A. Mozhaev, A. Varakin, K. Maslakov, P. Nikulshin, Comparison of citric acid and glycol effects on the state of active phase species and catalytic properties of CoPMo/Al2O3 hydrotreating catalysts, Appl. Catal. B: Environ. 205 (2017) 93–103.

[3] A. Stanislaus, A. Marafi, M.S. Rana, Recent advances in the science and technology of ultra low sulfur diesel (ULSD) production, Catal. Today 153 (2010) 1–68.

[4] J. Méndez, O.E. Franco-López, X. Bokhimi, D.A. Solís-Casados, L. Escobar-Alarcón, T.E. Klimova, Dibenzothiophene hydrodesulfurization with NiMo and CoMo catalysts supported on niobium-modified MCM-41, Appl. Catal. B: Environ. 219 (2017) 479–491.

[5] R.G. Leliveld, S.E. Eijsbouts, How a 70-year-old catalytic refinery process is still ever dependent on innovation, Catal. Today 130 (2008) 183–189.

[6] M. Breysse, G. Djega-Mariadassou, S. Pessayre, C. Geantet, M. Vrinat, G. Pérot, M. Lemaire, Deep desulfurization: reactions, catalysts and technological challenges, Catal. Today 84 (2003) 129–138.

[7] T. Fujikawa, H. Kimura, K. Kiriyama, K. Hagiwara, Development of ultra-deep HDS catalyst for production of clean diesel fuels, Catal. Today 111 (2006) 188–193.

[8] M. Trueba, S.P. Trasatti, γ-Alumina as a support for catalysts: a review of fundamental aspects, Eur. J. Inorg. Chem. 2005 (2005) 3393–3403.

[9] H. Topsøe, B.S. Clausen, N.Y. Topsøe, E. Pedersen, Recent basic research in hydrodesulfurization catalysis, Ind. Eng. Chem. Fundam. 25 (1986) 25–36.

[10] G. Berhault, M. Perez De la Rosa, A. Mehta, M.J. Yácaman, R.R. Chianelli, The single-layered morphology of supported MoS2-based catalysts-the role of the cobalt promoter and its effects in the hydrodesulfurization of dibenzothiophene, Appl. Catal. A: Gen. 345 (2008) 80–88.

[11] J.V. Lauritsen, S. Helveg, E. Lægsgaard, I. Stensgaard, B.S. Clausen, H. Topsøe, F. Besenbacher, Atomic-scale structure of Co-Mo-S nanoclusters in hydrotreating catalysts, J. Catal. 197 (2001) 1–5.

[12] F. Besenbacher, M. Brorson, B.S. Clausen, S. Helveg, B. Hinnemann, J. Kibsgaard, J.V. Lauritsen, P.G. Moses, J.K. Nørskov, H. Topsøe, S.T.M. Recent, DFT and HAADF-STEM studies of sulfide-based hydrotreating catalysts: insight into mechanistic, structural and particle size effects, Catal. Today 130 (2008) 86–96.

[13] Y. Okamoto, K. Ochiai, M. Kawano, T. Kubota, Evaluation of the maximum potential activity of Co-Mo/Al2O3 catalysts for hydrodesulfurization, J. Catal. 222 (2004) 143–151.

[14] J.V. Lauritsen, J. Kibsgaard, G.H. Olesen, P.G. Moses, B. Hinnemann, S. Helveg, J.K. Nørskov, B.S. Clausen, H. Topsøe, E. Lægsgaard, F. Besenbacher, Location and coordination of promoter atoms in Co- and Ni-promoted MoS2-based hydrotreating catalysts, J. Catal. 249 (2007) 220–233.

[15] E.J.M. Hensen, P.J. Kooyman, Y. van der Meer, A.M. van der Kraan, V.H.J. de Beer, J.A.R. van Veen, R.A. van Santen, The relation between morphology and hydrotreating activity for supported MoS2 particles, J. Catal. 199 (2001) 224–235.

[16] M.W.J. Crajé, S.P.A. Louwers, V.H.J. De Beer, R. Prins, A.M. Van der Kraan, An EXAFS study on the so-called cobalt-molybdenum-sulfur phase in cobalt/carbon and cobalt-molybdenum/carbon, compared with a Moessbauer emission spectroscopy study, J. Phys. Chem. 96 (1992) 5445–5452.

[17] T. Fujikawa, Development of new CoMo HDS catalyst for ultra-low sulfur diesel fuel production, J. Jpn. Pet. Inst. 50 (2007) 249–261.

[18] J.A. Bergwerff, T. Visser, G. Leliveld, B.D. Rossenaar, K.P. de Jong, B.M. Weckhuysen, Envisaging the physicochemical processes during the preparation of supported catalysts: Raman microscopy on the impregnation of Mo onto Al2O3 extrudates, J. Am. Chem. Soc. 126 (2004) 14548–14556.

[19] S. Eijsbouts, L.C.A. van den Oetelaar, R.R. van Puijenbroek, MoS2 morphology and promoter segregation in commercial Type 2 Ni-Mo/Al2O3 and Co-Mo/Al2O3 hydroprocessing catalysts, J. Catal. 229 (2005) 352–364.

[20] Y. Okamoto, K. Hioka, K. Arakawa, T. Fujikawa, T. Ebihara, T. Kubota, Effect of sulfidation atmosphere on the hydrodesulfurization activity of SiO2-supported Co-Mo sulfide catalysts: local structure and intrinsic activity of the active sites, J. Catal. 268 (2009) 49–59.

[21] S. Texier, G. Berhault, G. Pérot, V. Harlé, F. Diehl, Activation of alumina-supported hydrotreating catalysts by organosulfides: comparison with H2S and effect of different solvents, J. Catal. 223 (2004) 404–418.

[22] L.G. Woolfolk, C. Geantet, L. Massin, D. Laurenti, J.A. De los Reyes, Solvent effect over the promoter addition for a supported NiWS hydrotreating catalyst, Appl. Catal. B: Environ. 201 (2017) 331–338.

[23] A. Alsalme, N. Alzaqri, A. Alsaleh, M.R.H. Siddiqui, A.A. lotaibi, E.F. Kozhevnikova, I. Kozhevnikov, Efficient NiMo hydrodesulfurization catalyst prepared through Keggin polyoxometalate[J], Appl. Catal. B: Environ. 182 (2016) 102–108.

[24] S.K. Maity, J. Ancheyta, L. Soberanis, F. Alonso, M.E. Llanos, Alumina–titania binary mixed oxide used as support of catalysts for hydrotreating of Maya heavy crude, Appl. Catal. A: Gen. 244 (2003) 141–153.

[25] Y. Fan, X. Bao, H. Wang, C. Chen, G. Shi, A surfactant-assisted hydrothermal deposition method for preparing highly dispersed W/[gamma]-Al2O3 hydrodenitrogenation catalyst, J. Catal. 245 (2007) 477–481.

[26] W. Han, P. Yuan, Y. Fan, G. Shi, H. Liu, D. Bai, X. Bao, Preparation of supported hydrodesulfurization catalysts with enhanced performance using Mo-based inorganic-organic hybrid nanocrystals as a superior precursor, J. Mater. Chem. 22 (2012) 25340–25353.

[27] O.V. Klimov, A.V. Pashigreva, M.A. Fedotov, D.I. Kochubey, Y.A. Chesalov, G.A. Bukhtiyarova, A.S. Noskov, Co-Mo catalysts for ultra-deep HDS of diesel fuels prepared via synthesis of bimetallic surface compounds, J. Mol. Catal. A: Chem. 322 (2010) 80–89.

[28] L. Coulier, G. Kishan, J.A.R. van Veen, J.W. Niemantsverdriet, Influence of support-interaction on the sulfidation behavior and hydrodesulfurization activity of Al2O3-supported W, CoW, and NiW model catalysts, J. Phys. Chem. B 106 (2002) 5897–5906.

[29] G. Kishan, J.A.R. van Veen, J.W. Niemantsverdriet, Realistic surface science models of hydrodesulfurization catalysts on planar thin-film supports: the role of chelating agents in the preparation of CoW/SiO2 atalysts, Top. Catal. 29 (2004) 103–110.

[30] H. Li, M. Li, Y. Chu, F. Liu, H. Nie, Essential role of citric acid in preparation of efficient NiW/Al2O3 HDS catalysts, Appl. Catal. A: Gen. 403 (2011) 75–82.

[31] P. Mazoyer, C. Geantet, F. Diehl, S. Loridant, M. Lacroix, Role of chelating agent on the oxidic state of hydrotreating catalysts, Catal. Today 130 (2008) 75–79.

[32] M.A. Lélias, J. van Gestel, F. Maug, J.A.R. van Veen, Effect of NTA addition on the formation, structure and activity of the active phase of cobalt-molybdenum sulfide hydrotreating catalysts, Catal. Today 130 (2008) 109–116.

[33] D. Nicosia, R. Prins, The effect of glycol on phosphate-doped CoMo/Al2O3 hydrotreating catalysts, J. Catal. 229 (2005) 424–438.

[34] S.V. Budukva, O.V. Klimov, A.S. Noskov, A new method for reactivating the supported deep hydrotreatment CoMo/Al2O3 and NiMo/Al2O3 catalysts after oxidative regeneration, Catal. Ind. 7 (2015) 214–220.

[35] A. Cho, J.J. Lee, J.H. Koh, A. Wang, S.H. Moon, Performance of NiMoS/Al2O3 prepared by sonochemical and chemical vapor deposition methods in the hydrodesulfurization of dibenzothiophene and 4,6-dimethyldibenzothiophene, Green Chem. 9 (2007) 620–625.

[36] I. Bezverkhyy, P. Afanasiev, M. Lacroix, Promotion of highly loaded MoS2/Al2O3 hydrodesulfurization catalysts prepared in aqueous solution, J. Catal. 230 (2005) 133–139.

[37] L.G. Woolfolk, C. Geantet, L. Massin, D. Laurenti, J.A. De los Reyes, Solvent effect over the promoter addition for a supported NiWS hydrotreating catalyst, Appl. Catal. B: Environ. 201 (2017) 331–338.

[38] Y. Zhang, W. Han, X. Long, H. Nie, Redispersion effects of citric acid on CoMo/γ-Al2O3 hydrodesulfurization catalysts, Catal. Commun. 82 (2016) 20–23.

[39] C. Lamonier, C. Martin, J. Mazurelle, V. Harl, D. Guillaume, E. Payen, Molybdocobaltate cobalt salts: new starting materials for hydrotreating catalysts, Appl. Catal. B: Environ. 70 (2007) 548–556.

[40] M. Yin, F. Jia, F. Qiao, P. Zheng, W. Zhang, Y. Fan, Facile wet-chemical synthesis and efficient photocatalytic hydrogen production of amorphous MoS3 sensitized by Erythrosin B, Mater. Charact. 128 (2017) 148–155.

[41] L. Yu, B.Y. Xia, X. Wang, X.W. Lou, General formation of M-MoS3 (M = Co, Ni) hollow structures with enhanced eectrocatalytic activity for hydrogen evolution, Adv. Mater. 28 (2016) 92–97.

[42] B. Liu, Z. Jin, L. Bai, J. Liang, Q. Zhang, N. Wang, C. Liu, C. Wei, Y. Zhao, X. Zhang, Molybdenum-supported amorphous MoS3 catalyst for efficient hydrogen evolution in solar-water-splitting devices, J. Mater. Chem. A 4 (2016) 14204–14212.

[43] T. Weber, J.C. Muijsers, J.W. Niemantsverdriet, Structure of amorphous MoS3, J. Phys. Chem. 99 (1995) 9194–9200.

[44] K.S. Liang, S.P. Cramer, D.C. Johnston, C.H. Chang, A.J. Jacobson, J.P. deNeufville, R.R. Chianelli, Amorphous MoS3 and WS3, J. Non-Cryst. Solids 42 (1980) 345–356.

[45] M. De Boer, A.J. Van Dillen, D.C. Koningsberger, J.W. Geus, The structure of well defined SiO2 supported MoO3 clusters during sulfidation. An in situ EXAFS-study, Jpn. J. Appl. Phys. 32 (1993) 460–462.

[46] M. Tang, H. Ge, W. Fan, G. Wang, Z. Lyu, X. Li, Presulfidation and activation mechanism of Mo/Al2O3 catalyst sulfided by ammonium thiosulfate, Korean J. Chem. Eng. 31 (2014) 1368–1376.

[47] J.n.L. Brito, F. Severino, N. Ninoska Delgado, J. Laine, HDS activity of carbon-supported Ni-Mo catalysts derived from thiomolybdate complexes, Appl. Catal. A: Gen. 173 (1998) 193–199.

[48] W. Han, H. Nie, X. Long, M. Li, Q. Yang, D. Li, Effects of the support Brønsted acidity on the hydrodesulfurization and hydrodenitrogention activity of sulfided NiMo/Al2O3 catalysts, Catal. Today 292 (2017) 58–66.

[49] W. Han, H. Nie, X. Long, M. Li, Q. Yang, D. Li, Preparation of F-doped MoS2/Al2O3 catalysts as a way to understand the electronic effects of the support Brønsted acidity on HDN activity, J. Catal. 339 (2016) 135–142.

[50] W. Han, H. Nie, X. Long, M. Li, Q. Yang, D. Li, A study on the origin of the active sites of HDN catalysts using alumina-supported MoS3 nanoparticles as a precursor, Catal. Sci. Technol. 6 (2016) 3497–3509.

[51] G. Shi, W. Han, P. Yuan, Y. Fan, X. Bao, Sulfided Mo/Al2O3 hydrodesulfurization catalyst prepared by ethanol-assisted chemical deposition method, Chin. J. Catal. 34 (2013) 659–666.

[52] T. Huang, J. Xu, Y. Fan, Effects of concentration and microstructure of active phases on the selective hydrodesulfurization performance of sulfided CoMo/Al2O3 catalysts, Appl. Catal. B: Environ. 220 (2018) 42–56.

[53] J. Xu, T. Huang, Y. Fan, Highly efficient NiMo/SiO2-Al2O3 hydrodesulfurization catalyst prepared from gemini surfactant-dispersed Mo precursor, Appl. Catal. B: Environ. 203 (2017) 839–850.

[54] J.V. Lauritsen, J. Kibsgaard, S. Helveg, H. Topsoe, B.S. Clausen, E. Laegsgaard, F. Besenbacher, Size-dependent structure of MoS2 nanocrystals, Nat. Nanotechnol. 2 (2007) 53–58.

[55] S.J. Hibble, R.I. Walton, D.M. Pickup, A.C. Hannon, Amorphous MoS3: clusters or chains? The structural evidence, J. Non-Cryst. Solids 232–234 (1998) 434–439.

[56] H.G.S. Casalongue, J.D. Benck, C. Tsai, R.K.B. Karlsson, S. Kaya, M.L. Ng, L.G.M. Pettersson, F. Abild-Pedersen, J.K. Nørskov, H. Ogasawara, T.F. Jaramillo, A. Nilsson, Operando characterization of an amorphous molybdenum sulfide nanoparticle catalyst during the hydrogen evolution reaction, J. Phys. Chem. C 118 (2014) 29252–29259.

[57] Y. Fan, H. Xiao, G. Shi, H. Liu, Y. Qian, T. Wang, G. Gong, X. Bao, Citric acid-assisted hydrothermal method for preparing NiW/USY-Al2O3 ultradeep hydrodesulfurization catalysts, J. Catal. 279 (2011) 27–35.

[58] L. Qiu, G. Xu, Peak overlaps and corresponding solutions in the X-ray photoelectron spectroscopic study of hydrodesulfurization catalysts, Appl. Surf. Sci. 256 (2010) 3413–3417.

[59] W. Fu, L. Zhang, D. Wu, M. Xiang, Q. Zhuo, K. Huang, Z. Tao, T. Tang, Mesoporous zeolite-supported metal sulfide catalysts with high activities in the deep hydrogenation of phenanthrene, J. Catal. 330 (2015) 423–433.

[60] B. Guichard, M. Roy-Auberger, E. Devers, C. Legens, P. Raybaud, Aging of Co(Ni) MoP/Al2O3 catalysts in working state, Catal. Today 130 (2008) 97–108.

[61] F. Bataille, J.-L. Lemberton, P. Michaud, G. Pérot, M. Vrinat, M. Lemaire, E. Schulz, M. Breysse, S. Kasztelan, Alkyldibenzothiophenes hydrodesulfurization-promoter effect, reactivity, and reaction mechanism, J. Catal. 191 (2000) 409–422.

[62] Y. Li, D. Pan, C. Yu, Y. Fan, X. Bao, Synthesis and hydrodesulfurization properties of NiW catalyst supported on high-aluminum-content, highly ordered, and hydrothermally stable Al-SBA-15, J. Catal. 286 (2012) 124–136.

[63] G. Alonso, M. Del Valle, J. Cruz, V. Petranovskii, A. Licea-Claverie, S. Fuentes, Preparation of MoS2 catalysts by in situ decomposition of tetraalkylammonium thiomolybdates, Catal. Today 43 (1998) 117–122.

[64] J.L. Brito, M. Ilija, P. Hernández, Thermal and reductive decomposition of ammonium thiomolybdates, Thermochim. Acta 256 (1995) 325–338.

[65] S.J. Hibble, G.B. Wood, Modeling the structure of amorphous MoS3: a neutron diffraction and reverse monte carlo study, J. Am. Chem. Soc. 126 (2004) 959–965.

[66] C.H. Chang, S.S. Chan, Infrared and raman studies of amorphous MoS3 and poorly crystalline MoS2, J. Catal. 72 (1981) 139–148.

[67] M.L. Tang, D.C. Grauer, B. Lassalle-Kaiser, V.K. Yachandra, L. Amirav, J.R. Long, J. Yano, A.P. Alivisatos, Structural and electronic study of an amorphous MoS3 hydrogen-generation catalyst on a quantum-controlled photosensitizer, Angewandte Chemie 123 (2011) 10385–10389.

[68] P. Afanasiev, I. Bezverkhy, Synthesis of MoSx (5 > x > 6) amorphous sulfides and their use for preparation of MoS2 monodispersed microspheres, Chem. Mater. 14 (2002) 2826–2830.

[69] K.H. Hu, Y.R. Wang, X.G. Hu, H.Z. Wo, Preparation and characterisation of ball-like MoS2 nanoparticles, Mater. Sci. Technol. 23 (2007) 242–246.

[70] M. Nath, A. Govindaraj, C.N.R. Rao, Simple synthesis of MoS2 and WS2 nanotubes, Adv. Mater. 13 (2001) 283–286.